Available online at www.sciencedirect.com
ScienceDirect
Nuclear Instruments and Methods in Physics Research B 266 (2008) 998–1011
NIM B
Beam Interactions with Materials & Atoms
www.elsevier.com/locate/nimb

Rutherford backscattering using electrons as projectiles: Underlying principles and possible applications

M.R. Went, M. Vos *

Atomic and Molecular Physics Laboratories, Research School of Physical Sciences and Engineering, The Australian National University, Canberra 0200, Australia

Received 12 November 2007; received in revised form 20 January 2008
Available online 5 February 2008

Abstract

Ion beam analysis is the method of choice for studying the composition of layers with a thickness exceeding several tens of Å. Recently it has become clear that elastic scattering of keV electrons can be used to determine the surface composition of relatively thick layers (up to 1000 Å) in a way very similar to ion scattering experiments. These electron-scattering experiments share much of the underlying physics of electron spectroscopy and ion scattering. In this paper we systematically describe the similarities and differences between the electron-scattering experiments and the ion-beam experiments and illustrate this description with relevant electron-scattering examples.

PACS: 25.30.Bf; 82.80.Yc; 68.49.Jk

Keywords: Electron-scattering; Rutherford backscattering; Surface analysis

1. Introduction

Ion scattering has been used to study surfaces for around half a century [1]. These experiments are easy to interpret. At high energies the energy transfer from the projectile to the target is, for almost all events, dominated by a single collision between the projectile and a specific target atom. The energy transfer between projectile and target atoms depends on the mass and the scattering angle θ and is described by the kinematic factor: $k = E_1/E_0$ with E_0, E_1 the energy of the projectile before and after scattering. The largest energy transfer is for backscattering ($\theta = 180°$) and then $k = (M_2 - M_1)^2/(M_1 + M_2)^2$ with M_1, M_2 the mass of the projectile and scatterer respectively. Thus, for example, for a He ion scattering from Si through 180° one obtains $k = 0.56$, i.e the He ion loses almost half its energy. If one uses the same equation for backscattering of electrons, then one obtains for an electron-scattering through 180° from Si an extremely small change in kinetic energy ($k = 0.99992$) and any attempt to use this extremely small reduction in energy to obtain information about the target composition, appears ill-conceived. The maximum energy loss for a 40 keV electron backscattering from Si would be 3.2 eV. This energy loss is, however, large when compared to the resolution in high-energy electron energy-loss spectroscopy, where a resolution of a few 100 meV is obtained routinely, even at several 100's of keV of primary energy [2], indicating that it is conceivable that an electron backscattering experiment could be successful. In this paper we will show that it is indeed possible to obtain information from scattered electrons, in a fashion that resembles in many ways Rutherford backscattering using ions. We will refer to this technique using the acronym ERBS: electron Rutherford backscattering.

Besides the kinematic factor being close to 1, there is a host of other issues that have to be addressed in order to be able to interpret data of backscattered electrons. For example:

* Corresponding author.
E-mail address: maarten.vos@anu.edu.au (M. Vos).

0168-583X/$ - see front matter © 2008 Elsevier B.V. All rights reserved.
doi:10.1016/j.nimb.2008.01.059

- Can we interpret the interaction of an electron with the target as the collision between a single atom and an electron, or should we describe it within the framework of electron diffraction.
- Is it possible to calculate the energy transfer between projectile and scattering atom, without considering the fact that the atom is bound to a lattice, especially if the energy transfer is smaller than the binding energy of the atom.
- What happens if the projectile creates inelastic (electronic) excitations in the target and what determines the depth resolution of these experiments.

It will turn out that in some respects backscattering of electrons is fairly close to ion beam analysis, but in other respects the technique resembles electron spectroscopies such as XPS. Most of the papers published on ERBS approach the technique from the viewpoint of electron spectroscopy, see e.g. [3,4]. Here we approach the technique from an ion scattering background, whenever possible. A comparison of ERBS to neutron Compton scattering, focussing on hydrogen detection, was published before and covers many of the issues raised here, using neutron physics as a background [5].

This paper is organized as follows: we first describe the experimental apparatus used, then present spectra obtained and interpret these spectra. Some of the underlying theory is quite involved. Here we present the results of the measurements and use the experimental outcome as a justification for the interpretation. We will refer to more general scattering literature for the theoretical underpinning.

We will see that, in almost all cases, information on the surface composition is obtained only from electrons that are scattered without creating electronic excitations. The mean free path for the creation of inelastic excitations determines the depth scale probed by the experiment. However, the electrons that are backscattered after creating electronic (inelastic) excitations in the sample should be interpreted as in reflection electron energy-loss spectroscopy (REELS). These electrons carry information on the electronic structure of the overlayer. Only in special cases, where the energy width of the electronic excitations is smaller than the separation of the different elastic peaks, do these electrons contain information on the depth distribution of the scatterers. Thus we will show that this method straddles the fields of electronic spectroscopy and ion scattering and reveals a rather unique set of information.

2. Experimental setup

Energy resolution is of crucial importance in these experiments. A highly mono-energetic beam is required, followed by an analyzer with high resolving power. The spectrometer is equipped with 2 electron guns, each with a barium oxide cathode, as this is an emitter with a low work function, operating at a low temperature and hence small thermal spread. The electron gun is at a potential

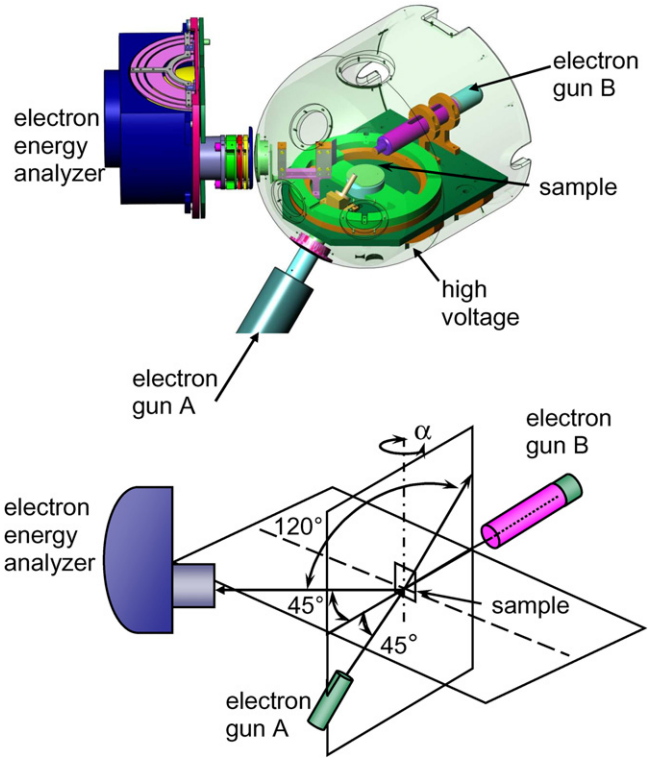

Fig. 1. The main parts of the spectrometer are displayed in the top half, showing the analyzer and the high voltage sphere, as well as the direction of the incoming and outgoing electron beams. The lower half illustrates the angles in the experiment. If we use gun A, then the sample is in the orientation shown ($\alpha = 0°$), if we use gun B for thick samples then the sample is rotated to $\alpha = 112.5°$.

of −500 V, derived from a power supply with drift and ripple smaller than 50 meV. If gun A is used (see Fig. 1) then the scattering angle θ is 120° . For gun B the scattering angle θ is 45°. The sample is in contact and surrounded by a metal semi-sphere kept at a high voltage (up to 39.5 keV). Thus incoming electrons are accelerated (and focussed) while entering the high voltage region. In this way a beam of electrons with an energy up to 40 keV and intensity of a few nA impinges on the sample (spot size diameter 0.2–0.4 mm). Those electrons emerging at the desired scattering angle θ are detected by an electrostatic analyzer. This hemispherical analyzer operates at a pass energy of 200 eV and hence, when measuring the elastic peak is at a potential near −300 V (the difference of the gun and analyzer potential corresponds to the pass energy). Thus the scattered electrons entering the analyzer are decelerated from the high-energy down to a kinetic energy of approximately 200 eV. This is accomplished by a set of slit lenses. The lenses not only decelerate the electrons but also form an image of the beam spot on the sample at the entrance plane of the hemispherical analyzer. At the exit plane of the hemispherical analyzer there is a position sensitive detector, allowing electrons within an energy window of 30 eV to be detected simultaneously. Good quality spectra are obtained in an hour. The advantage of this setup is that the main high voltage supply can have ripple and drift

considerably larger than the experimental resolution without affecting the outcome of the experiment, as it both accelerates and decelerates the detected electrons. Also the position sensitive detector (two channel plates followed by a resistive anode) is relatively close to ground in this configuration, facilitating the readout of the pulses by a data acquisition system.

3. Diffraction versus collisions, mass separation and impulse approximation

The interaction of electrons impinging on a thin film is sometimes described by diffraction (e.g. in a transmission electron microscope) and sometimes as a collision between the electrons and a nucleus (e.g. when describing Frenkel pair production by electrons with energy of the order of 1 MeV (see e.g. [6])). What is the right way to describe the current experiment?

Within the first approach (diffraction) the electron is described as a wave interacting with all atoms and the change in momentum of the impinging electron is absorbed by the whole of the crystal. If an electron with momentum $\boldsymbol{k_0}$ is deflected over an angle θ by a scatterer with a mass much larger than the electron mass, then the change in momentum of the electron is given by $q = 2k_0 sin(\theta/2)$ (see Fig. 2). In the case of diffraction the energy transfer to the target, is thus $q^2/2M_c$ with M_c the mass of the crystal. As the crystal is considered to be large ($M_c = \infty$), this energy transfer would approach 0. In the second approach the electron is assumed to interact with a single atom (with mass M_a) and the transferred energy $q^2/2M_a$, is small but finite. We refer to this energy as the mean recoil energy $\overline{E_r}$ (why we call this quantity the mean recoil energy will become clear later). A different, but equivalent expression for the kinematic factor is then: $k = (E_0 - \overline{E_r})/E_0$. The maximum energy transfer occurs for scattering through 180° (when $\boldsymbol{q} = 2\boldsymbol{k}_0$) and is given by $\overline{E_r} = 2k_0^2/M_a$. The scattering is then described as scattering by a free atom, the fact that the atom is part of a crystal is tacitly assumed not to influence the outcome.

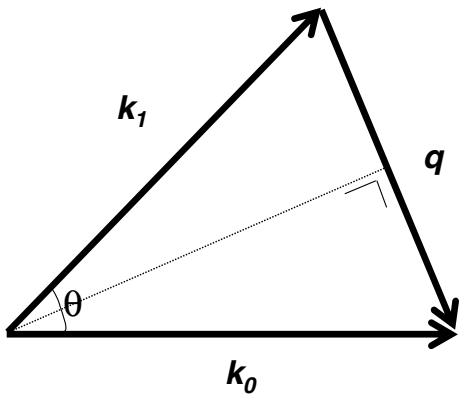

Fig. 2. The relation between momentum transfer and scattering geometry. If the energy loss in the collision is much smaller than the incoming energy E_0 then the magnitude of the incoming momentum $|k_0|$ is approximately equal to the magnitude of the outgoing momentum $|k_1|$ and the magnitude of the momentum transfer $\boldsymbol{q}$ equals $2k_0 \sin\theta/2$.

Thus by carefully measuring the energy of the scattered electron we can determine experimentally if the electron is scattered by a single atom or the crystal as a whole. Indeed the question about diffraction versus scattering was answered in this way by Boersch et al. in the 60's [7]. They were able, using 30 keV electrons scattering through 90°, to resolve a shift of the elastic-scattering peak for electrons scattered from carbon, which appeared consistent with scattering from a free carbon atom. They concluded that the elastically scattered electron was deflected by a single carbon atom, and explained the observed energy shift by assuming that this carbon atom acquired a kinetic energy $q^2/2M_a$. Similar results were obtained in more recent days, at lower primary energies, but better energy resolution [8–10]. Because of the reduction in the kinetic energy of the electrons, these experiments are sometimes referred to as 'quasi-elastic' scattering experiments. Such recoil effects play a role in both electron-scattering and high-energy photoemission and different theoretical approaches were presented by several authors [11–14].

The reason why at large energy and scattering angle an electron interacts with a single atom and not diffract from the crystal, is the high momentum transfer in these collisions. The waves emanating from different atoms a and b have a phase difference given by $e^{-i\boldsymbol{q}\cdot\boldsymbol{r}}$, with $\boldsymbol{r}$ the relative position of atom a to atom b. For large momentum transfer $\boldsymbol{q}$ the phase factor varies extremely rapidly with $\boldsymbol{r}$. As $\boldsymbol{r}$ varies due to vibrations (even at 0 K we have zero-point motion), diffraction effects average out to 0 and we are left with scattering from single atoms. This is sometimes referred to as the incoherent approximation. See e.g. [15] for a discussion of the incoherent approximation within the context of neutron scattering.

Repeating the experiments with a modern spectrometer and at high energies reveals the energy transfer very clearly. In Fig. 3 we show the spectra of electrons scattered at 40 keV and 20 keV through 120° from a carbon film (i.e. using gun A in Fig. 1). As the exact determination of the zero energy loss position of the spectrometer is somewhat complicated we evaporated some Au atoms onto the carbon. The spectra show two clear peaks (only one peak was observed before gold evaporation). The peak at low energy loss is assumed to be due to Au and the zero of the energy scale is adjusted such that this peak is at $q^2/2M_{Au}$. The separation of these peaks was calculated assuming scattering from free Au and C atoms and this separation is indicated as well. Agreement for the 120° measurement is very good. Note that in order to calculate the separation, one can not simply use an energy-independent kinematic factor, as is done in ion scattering [1], as the energy of a 40 keV electron is not negligible compared to its rest mass (≈511 keV). This causes an enhancement in the energy transferred from the electron to the nucleus by a factor $1 + E_0/1022$ with E_0 the electron energy in keV. Inclusion of this correction factor (4% at 40 keV) does

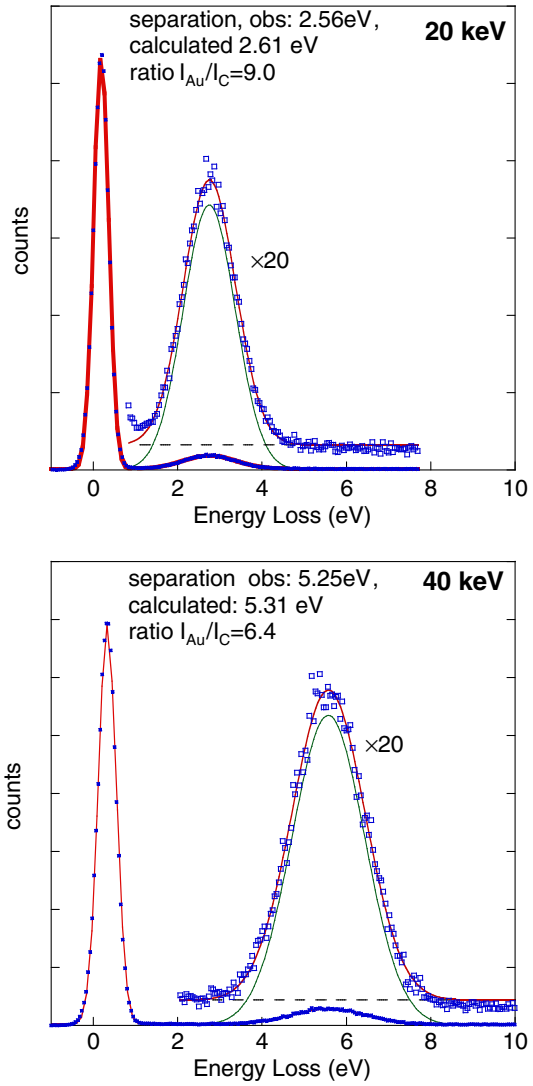

Fig. 3. Spectra from electrons backscattered from a carbon film on which $\simeq 4$ Å Au was deposited ($E_0 = 20$ keV (top) and $E_0 = 40$ keV (bottom)). The intense peak is due to electrons scattered elastically from Au, the broad, less intense peak is due to electrons scattered elastically from C. The fit (red line) consisted of 2 Gaussians and a Shirley background (dashed line). The thin line is the Gaussian corresponding to the carbon peak, without background. (For interpretation of the references to colour in this figure legend, the reader is referred to the web version of this article.)

improve agreement between experimentally obtained and calculated separations noticeably.

Thus even in these collisions, where the transferred energy is much smaller than the energy required to create a Frenkel pair it appears that the energy transfer is well described assuming scattering by a free atom. This approximation is expected to become better at higher recoil energies. Thus these experiments can be seen as a direct experimental verification of the (often implicit) assumption that the Frenkel pair formation energy is equal to the maximum energy transferred from an electron to a free atom at the threshold energy.

The approximation assuming that the collision between the projectile and target atom can be described as a collision between free particles is often referred to as the impulse approximation. For collisions with an energy transfer of a few eV this approximation has been extensively studied in neutron scattering research [15] and deviations are found at low energy transfer. One way of understanding why this approximation works, even when the transferred energy is less than the lattice binding energy, is by considering the time scale of the collision. The collision is very fast (10^{-15} s) and during this time the target atom hardly moves, hence it does not 'feel' the effect of the surrounding atoms [15].

4. Doppler broadening

Besides the splitting of the Au and C elastic peaks it is also obvious from Fig. 3 that the Au and C peaks have completely different widths. The Au peak is narrow, compared to the C peak. One possible explanation would be that multiple scattering is important: electrons backscatter sometimes in a single collision and sometimes by a series of collisions. For trajectories where multiple scattering occurs the total energy transferred to the target would be $\sum_i q_i^2/2M_a$ with $\boldsymbol{q}_i$ the momentum transfer in collision i. This would lead to a range of possible energy transfers which could be the cause of the large width of the carbon peak.

In order to study the effects of multiple scattering, we performed transmission experiments through carbon film with thicknesses ranging from 90 Å to 1400 Å [16], using 40 keV electrons. The elastic mean free path of 40 keV electrons in carbon is ≈550 Å at 40 keV. In transmission experiments, the length of the trajectory is at least the film thickness. The probability of multiple scattering would thus be much larger for film thicknesses greater than the elastic mean free path, compared to films that are thinner than the elastic mean free path. However, at most a slight increase of the peak width with film thickness was found. Hence the large difference in peak width between Au and C elastic peak is not due to multiple scattering.

By far the most important cause of the difference in widths is Doppler broadening. Again we assume that the collision between the electron and the atom of the solid can be described as a collision between an electron and a free atom. If the atom has a momentum $\boldsymbol{p}$ before the collision, then after the collision it will have a momentum $\boldsymbol{p}+\boldsymbol{q}$. The recoil energy is then the difference in the kinetic energy of the atom before and after the collision. It is given by

$$E_r = \frac{(\boldsymbol{p}+\boldsymbol{q})^2}{2M_a} - \frac{p^2}{2M_a} = \frac{q^2}{2M_a} + \frac{\boldsymbol{p}\cdot\boldsymbol{q}}{M_a} \quad (1)$$

The first term is the mean recoil energy $\overline{E_r}$, the energy shift for scattering from a stationary atom and the second term describes the Doppler broadening of the recoil energy due to the motion of the atom before the collision. The Doppler

broadening is thus more important for scattering from a light atom (it is proportional to $1/M_a$) and indeed the carbon peak is much wider than the Au peak. Doubling the energy will approximately increase the momentum transfer (and hence the Doppler broadening) by $\sqrt{2}$. The carbon peak width (FWHM), obtained from the fitting procedure increases from 1.45 eV at 20 keV to 2.03 eV at 40 keV, a factor of 1.4 [17].

The Au peak width is mainly (but not exclusively) determined by experimental resolution and is found to be 0.41 eV at 20 keV and 0.50 eV at 40 keV.

In the low-temperature limit the Doppler broadening is determined by the zero-point motion of the atoms. Each phonon in the ground state has an energy of $\hbar\omega/2$; half of this will be kinetic energy and it is the corresponding momentum that is measured here. Doppler broadening will be larger for atoms in a stiff lattice (atoms well localized in coordinate space, hence by the Heisenberg uncertainty principle, their momentum-space wave function is delocalized). In the high temperature limit the atoms will behave like a classical gas and will have on average $3kT/2$ kinetic energy and the measured momentum distribution will reflect this temperature. The low-temperature limit is valid for $T \ll \Theta_d$, the high-temperature limit for $T \gg \Theta_d$ with Θ_d the Debye temperature.

Doppler broadening has been identified as one of the limitations on the maximum obtainable resolution in an medium-energy ion scattering (MEIS) experiments, see e.g. [18]. From Eq. (1) it is clear that the magnitude of the Doppler broadening is relatively large (compared to the average recoil energy) at low momentum transfer. This is the explanation of the fact that this effect is obvious in electron scattering, but difficult to resolve in ion scattering, as the momentum transfer is much larger in ion-scattering experiments.

For a harmonically bound isotropic solid, there is a simple relation between the Doppler width (FWHM) ΔE_{Dop} and the mean total kinetic energy $\langle E_{kin}\rangle$ [19,20]:

$$\Delta E_{Dop} = 2\sqrt{2\ln 2}\sqrt{(4/3)\langle E_{kin}\rangle E_r}. \quad (2)$$

Within the ion beam literature [18,21] Doppler broadening is usually discussed for (p,γ) reactions, in terms of the resonance energy E_{res} and then $E_r \approx (M_p/M_a)E_{res}$. Estimates of $\langle E_{kin}\rangle$ based on neutron Compton scattering vary from 108 meV in hydrogenated amorphous carbon [22] to 91 meV for poly-crystalline graphite [23]. Using an estimate of $\langle E_{kin}\rangle = 100$ meV we obtain a width ΔE_{Dop} of 1.44 eV at 20 keV and 2.04 eV at 40 keV in excellent agreement with the experimental values [17].

As is clear from Eq. (1) the Doppler shift is proportional to the momentum component of the target atom along the transferred momentum direction. If we use a highly oriented pyrolytic graphite (HOPG) we can study the anisotropy of the target-atom momentum distribution in graphite. At 45° scattering angle (i.e. using gun *B* in Fig. 1), it was possible to change the direction of $\boldsymbol{q}$ from perpendicular to parallel to the graphite planes, using a reflection and a transmission geometry. At 45° scattering angle the transferred momentum is smaller than for the 120° scattering angle, hence the carbon peaks are narrower and the energy separation of Au and C is smaller. However, as can be seen in Fig. 4, there is still a clear difference in the width of spectra with $\boldsymbol{q}$ along the graphite planes (larger width) compared to perpendicular to these planes (narrower). Thus the vibrational anisotropy was resolved. Note that there is also a small change of the separation of the Au and C peaks. This is a clear sign that the impulse approximation is not perfect for these experiments at smaller scattering angles i.e. smaller momentum transfer. For more details see [16].

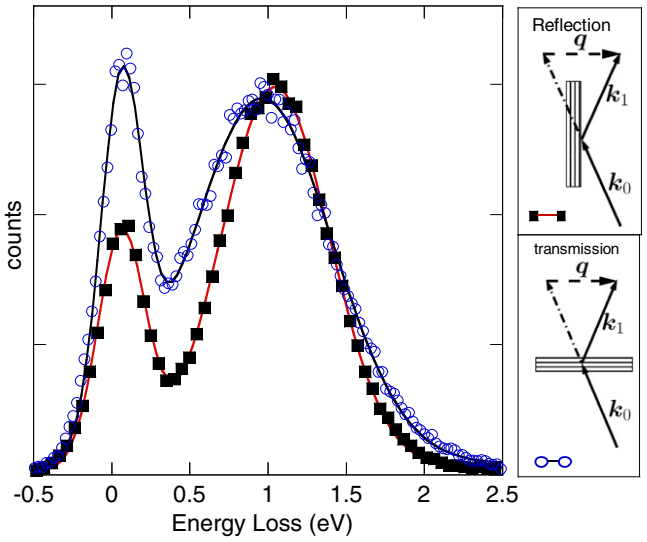

Fig. 4. Measurement of 40 keV electrons scattered through 45° from a HOPG sample on which some Au was deposited, in both a transmission and reflection geometry. The measurement geometry, as well as the direction of the transferred momentum relative to the graphite planes is sketched at the right.

5. Differential cross section for keV electron-scattering elastically by nuclei

The Au peak in Fig. 3 is much larger than the carbon peak, and from this one could conclude that the electrons do not penetrate the sample by much more than the thickness of the Au layer (≈ 4 Å). This is not true since at 20 and 40 keV the inelastic and elastic mean free paths are of the order of 100 Å. The difference in intensity is due to the large difference in the elastic scattering cross section of C and Au. This is well known from ion scattering where the cross section at MeV energies is given by the Rutherford formula and scales as Z^2.

If one describes (ion) Rutherford backscattering at MeV energies in semiclassical terms, then the impact parameter of these collisions is much smaller than the extent of the inner electron orbitals. Thus, effectively the ions scatter from a bare nucleus and because of this their cross section is given by the Rutherford formula. The Rutherford cross

section is proportional to Z^2 and decreases with energy $\propto (1/E_0)^2$. For electrons with energy of several 10's of keV, the classical impact parameter is, for heavy elements, larger than the radius of the inner orbitals and the electron scatters from a screened nucleus. The cross section will then not scale as Z^2 and $(1/E_0)^2$, but it can be calculated from the atomic charge distribution in a quantum mechanical approach, as is done in, for example, the ELSEPA package developed by Salvat et al. [24].

The most straightforward way to study the ratio of scattering cross sections of different elements is the study of well-defined compounds [25]. An example is given in Fig. 5 for the case of MoS_2. The Mo:S peak area expected based on the Rutherford formula is $42^2 : (2 \times 16^2) \simeq 3.4 : 1$. Indeed the ERBS spectrum taken at 40 keV energy and using a scattering angle of 120° displays two peaks. The separation of these peaks is 1.40 eV (the calculated value based on electrons scattering from free Mo and S is 1.41 eV) and the ratio of their intensities is 4.6 : 1. This is significantly different from the values obtained from the Rutherford formula. If we calculate the cross section, taking into account the electronic charge distribution, as calculated for free atoms, we obtain, using the ELSEPA package [24], an expected peak area ratio of 4.4 : 1. This is very close to the observed ratio. Note that in this case the screening enhances the Mo cross section at this particular angle and energy. This may seem somewhat contradictory from a semi-classical point of view, but it is a commonly occurring phenomenon [26].

Thus, except for the case were only light elements are involved, one can not describe the scattering cross section by the Rutherford formula. Screening of the nucleus by the core electrons has to be taken into account and inclusion of these effects improves agreement between experiment and theory greatly. One could see these electron-scattering experiment as an experimental way of testing theories describing the differential elastic cross section at high momentum transfer.

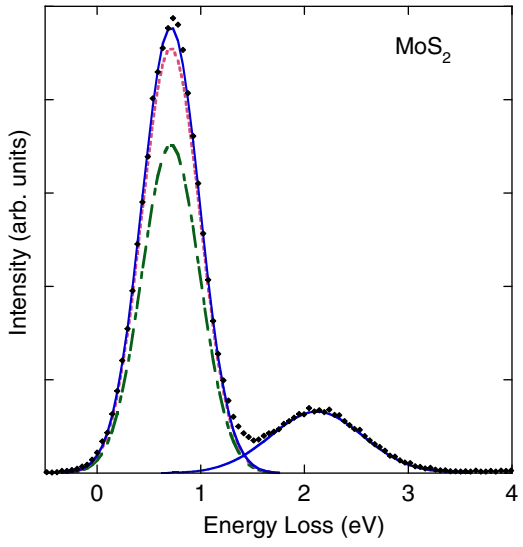

Fig. 5. The spectrum (dots, $E_0 = 40$ keV, $\theta = 120°$) from MoS_2 fitted with 2 Gaussians (solid lines). The component at ≈ 0.7 eV energy loss is due to Mo, the one near $\approx$2.1 eV is due to S. The dashed-dotted line is the expected size of the Mo elastic peak, relative to the S peak, if the Rutherford cross sections is assumed, the dotted line if the ELSEPA [24] cross section is assumed.

6. Probing depth

An important issue is the thickness of a sample that is probed in these experiment [17]. Experimentally, we can investigate this by using an overlayer, on a substrate of different mass, so two well-resolved contributions are observed. In practice the relative signal strength of the substrate layer (relative to the signal of the overlayer) is more important than the absolute intensity and often a value of 5% relative signal strength is considered as the maximum overlayer thickness for which the substrate is still detected. This thickness is then referred to as the probing depth. The actual probing depth varies greatly for different configurations. Let us again use the Au-C system to illustrate this.

The peaks shown in Fig. 3 are due to electrons that have not created electronic excitations in the target. These electrons have thus not lost energy due to electronic stopping. Electron trajectories are best described by discrete electronic excitations happening at certain places, not by a continuous loss of energy per unit distance traveled as is the custom for ion beams. The mean distance between electronic excitations is given by the inelastic mean free path λ_{in}. If the depth of the elastic scatterer is such that sum of the length of the incoming and outgoing trajectories is L, then the probability that an electron backscattered from this atom is detected without energy loss is proportional to $e^{-L/\lambda_{in}}$.

Not much direct experimental information about the inelastic mean free path λ_{in} exists for energies of 20–40 keV. Extrapolating the formulae developed for photoemission energies (up to a few keV) results in values at 40 keV of 637 Å for C and 246 Å for Au [27]. At 20 keV the obtained values are almost half these values (347 Å and 136 Å, respectively). Thus, if a Au surface is covered by a carbon layer, then, if the incoming and outgoing trajectories make an angle of 45° with the surface normal, the Au intensity will be halved at 40 keV for a C thickness of $637 \sin 45°/2 = 225$ Å.

Under these experimental conditions, the differential elastic-scattering cross section of Au is $\approx$ 360 times that of C. Thus for 225 Å C deposited on Au the Au peak will still be two orders of magnitude larger than the C peak and the Au peak will remain visible up to coverages of 1000 Å. For the reverse case only a few Å of Au deposited on C will completely dominate the spectrum. In Fig. 6 we illustrate this for an experiment using a 25 keV beam. Here the substrate signal is 5% of the overlayer signal; i.e. the overlayer thickness is equal to the probing depth. For the Au overlayer on C the probing depth is equal to the overlayer

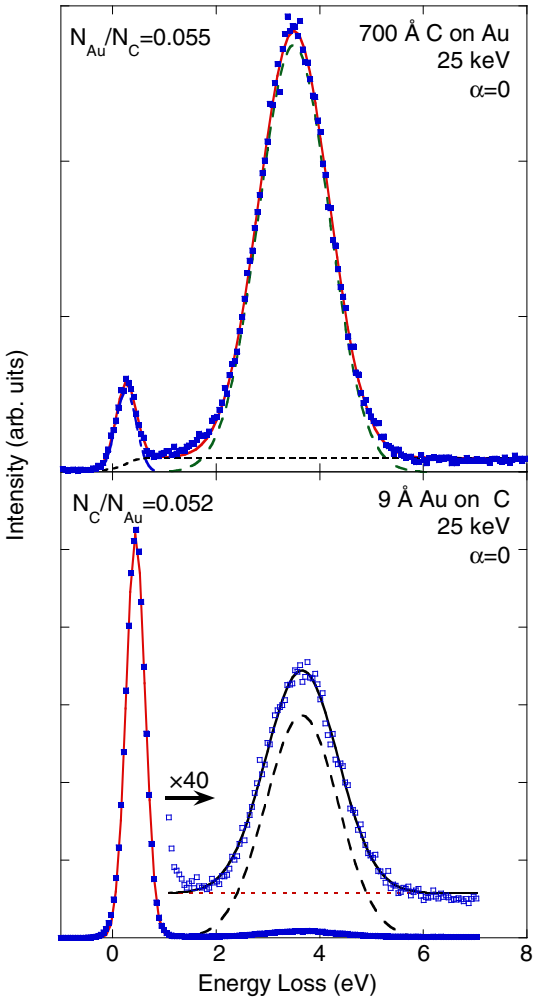

Fig. 6. Two samples for which the overlayer intensity is 95% of the substrate intensity. At 25 keV 700 Å of carbon is required for the overlayer intensity to be 20× that of the Au substrate. However, in the reverse case, only 9 Å of Au is required for the Au signal to be 20× that of the carbon substrate. Both incoming and outgoing beams made an angle of 45° with the surface normal.

thickness for an Au layer of only 9 Å, but for the reverse case a carbon thickness of 700 Å is required before the Au signal strength is diminished to 5%. Thus how deep these experiments 'see' is an interplay between the elastic scattering cross sections and the inelastic mean free path.

For a given sample one can increase the surface sensitivity by decreasing the incoming energy, or by making either the incoming or outgoing beam more glancing. The first approach reduces the peak separation and can only be used if the contributing peaks are well resolved at all energies.

7. Energy dependence of spectra of substrate-overlayer systems

Understanding the results for an inhomogeneous sample is more challenging. Often spectra taken at different primary energies are required to narrow down the possible number of interpretations. Changing the primary energies will affect both cross sections and the inelastic mean free path. As an example we discuss the spectra of a very small amount of Au and Ag evaporated on carbon (highly oriented pyrolytic graphite HOPG); the spectra were taken using electron energies between 7 and 40 keV. Relevant parameters are summarized in Table 1. Metals deposited on HOPG are well known to form islands, as the interaction between ad-atom and substrate is weak (see e.g. [28,29]) with a height of several nm. Thus attenuation of the beam at high primary energy in the metallic clusters is negligibly small, but for lower energies the combined length of the incoming and outgoing trajectories in a cluster can be comparable to the inelastic mean free path. The carbon signal is not affected by this, as it originates, in the large majority of events, from the part of the HOPG surface that is not covered by clusters. Thus interpretation is quite complex. After the electron-scattering experiment the samples were measured using conventional RBS as well (2 MeV He^+). The average thickness of the metal overlayers was found to be $N_{Ag} = 1.78 \pm 0.07 \times 10^{14}$ atoms/cm^2 (0.30 Å) for Ag and $N_{Au} = 0.80 \pm 0.03 \times 10^{14}$ atoms/cm^2 for Au (0.14 Å).

Spectra are shown in Fig. 7. Let us first compare the 40 keV electron spectrum to the ion RBS spectrum. Both RBS spectra were taken with the same integrated charge, as can be seen from the complete overlap of the carbon signal. The Ag:Au peak area is thus proportional to the $N_{Ag}\sigma_{Ag} : N_{Au}\sigma_{Au}$. The Au peak area was thus 1.27× larger than the Ag peak area. For ERBS the measurements were

Table 1
Properties relevant for interpretation of the metal/HOPG experiment

E_0 (keV)	C λ_{in} (Å)	Ag λ_{in} (Å)	Au λ_{in} (Å)	C $\overline{E_r}$ (Å)	Ag $\overline{E_r}$ (eV)	Au $\overline{E_r}$ (eV)	C $\frac{d\sigma}{d\Omega}$ (R) (cm^2)	C $\frac{d\sigma}{d\Omega}(E)$ (cm^2)	Ag $\frac{d\sigma}{d\Omega}(R)$ (cm^2)	Ag $\frac{d\sigma}{d\Omega}(E)$ (cm^2)	Au $\frac{d\sigma}{d\Omega}$ (R) (cm^2)	Au $\frac{d\sigma}{d\Omega}$ (E) (cm^2)
7	140	69	56	0.97	0.11	0.06	1.72E-21	1.69E-21	1.05E-19	1.43E-19	2.97E-19	2.54E-19
10	190	93	75	1.38	0.15	0.08	8.46E-22	8.26E-22	5.19E-20	7.25E-20	1.47E-19	1.60E-19
20	347	168	135	2.80	0.31	0.17	2.15E-22	2.02E-22	1.32E-20	1.81E-20	3.73E-20	6.10E-20
30	494	238	192	4.23	0.47	0.26	9.75E-23	9.02E-23	5.98E-21	7.94E-21	31.69E-20	2.98E-20
40	637	306	246	5.70	0.63	0.34	5.58E-23	5.03E-23	3.42E-21	4.38E-21	9.68E-21	1.76E-20

The calculated inelastic mean free paths using the TPP-2M formula [27], the mean recoil energy ($E_r = q^2/2M$) for scattering through 120° and the elastic scattering cross sections at this angle as obtained from the Rutherford formula (R) and the ELSEPA package (E) [24], for the relevant energies and elements. More recent result ([30]) give values of λ_{in} for C that are at all energies somewhat smaller (by about a factor of 1.5) than those given by [27].

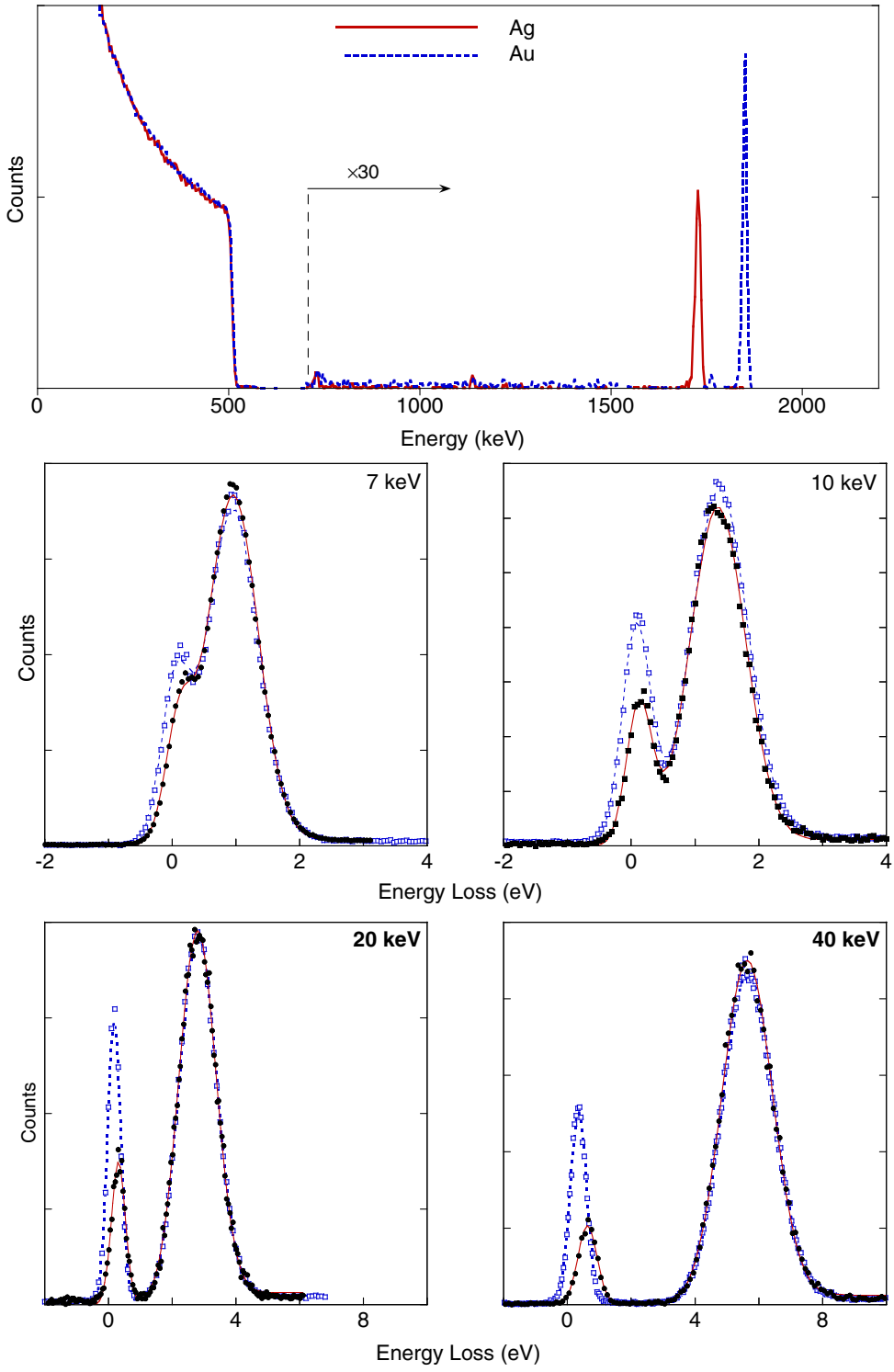

Fig. 7. Top panel: conventional RBS spectra (2 MeV He^+) of two HOPG samples on which a small amount of Ag and Au was deposited. The lower four panels show ERBS results for the same samples taken at energies as indicated (Ag – filled symbols, Au – open symbols).

taken with different amounts of integrated charge. We manually normalize both C peaks to the same area. Then the Au peak area is 2.4× the Ag peak area. This is almost a factor of 2 different from the RBS value and one possible explanation would be that the electron cross sections deviate significantly from the Rutherford values. If we use the calculated ELSEPA cross sections, then we would expect for these samples an Au peak that is 1.8× the Ag peak area. This is still 25% smaller than the observed ratio.

If we change the incoming energy from 40 to 20 keV we see that the signal of the overlayer becomes a larger

fraction of the carbon signal with decreasing energy. The thickness of the carbon layer that contributes to the carbon signal is proportional to the inelastic mean free path of the electrons in carbon. Both the Ag-on-C and Au-on-C spectra will be affected in the same way by changes in the carbon inelastic mean free path. If we plot the expected change in peak ratio due to the change in the inelastic mean free path, then we see that at energies above 20 keV the Ag:C intensity ratio is predicted fairly well (see Fig. 8). The increase in the Au:C ratio with decreasing energy is somewhat too low. We attribute this to screening. A change in primary energy will change both the C and metal differential cross section. If screening is not important (and the Rutherford formula applies) all cross sections will scale like $1/E_0^2$ and the ratio of the carbon to metal cross section would be energy independent. This is a fairly good approximation for Ag on C, but not for Au on C (see Table 1). The Au:C cross section ratio decreases with decreasing energy. This causes a reduction in the relative Au signal strength at low energies. In Fig. 8 we also plot the expected peak intensity ratio if both cross sections and carbon inelastic mean free path variations are taken into account. The agreement above 20 keV is now reasonable for both Au and Ag, but at 10 and 7 keV, esp. in the case of Ag the agreement is poor. We tentatively attribute this to island formation. The maximum (incoming plus outgoing) total path length in a metal cluster of a few nm becomes comparable with the inelastic mean free path of electrons in these metals at low energy and hence atoms buried deep in the clusters contribute less to the metal elastic peak. If this interpretation is correct, then an average cluster height of the order of 7 nm would be required to get an attenuation of the Ag signal by a factor of 2. This is somewhat larger than the cluster height often quoted in the literature (3 nm) [28,29]. The Au clusters would be smaller than the Ag clusters, as the deviation is smaller in the Au case. Whether clustering is responsible as well for the 25% disagreement obtained when comparing the 40 keV electron measurement with the ion RBS measurement is currently an open question.

8. Combined compositional analysis and electronic structure determination

In the previous section, we have restricted ourselves to the elastic peak. However these experiments always acquire spectra over a larger energy-loss range. Examples are shown in Fig. 9, for the case of Al deposition on sputter-cleaned polycrystalline Mo and Pt substrates. These experiments have been discussed at length elsewhere [31]; here we summarize the main points. In the left panel we show the elastic-peak part of the measured spectra. After Al deposition, its elastic peak is visible as an extremely small peak near 2 eV energy loss. This peak is small because the elastic-scattering cross section of Al is much smaller than that of Mo. Thus almost all detected electrons scattered elastically from Mo. Much more significant is the change in the energy-loss spectra. The inelastic mean free path of 40 keV electrons in Al is ≈ 530 Å [27]. The incoming and outgoing trajectories make an angle of 45° with the surface normal, hence there is a ≈ 35% chance that these electrons create an inelastic excitation in the 80 Å thick Al overlayer (assuming that Al is deposited as a continuous layer). Indeed a sharp peak is seen in the loss spectra at 15.2 eV below the Mo elastic peak, which we interpret as Al bulk plasmon excitation. Double plasmon excitation (visible in the energy loss spectra of pure Al near 30 eV) is not seen, as the probability that 2 plasmons are created in such a thin Al layer is still small. The observed

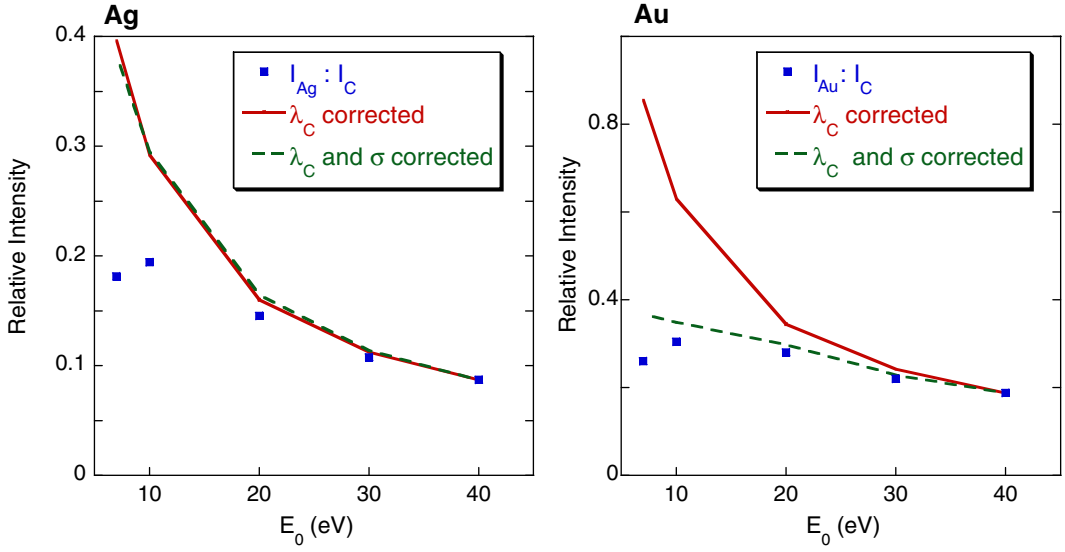

Fig. 8. The metal-to-carbon peak area ratio for different energies for ≈ 0.1 Å Ag and Au evaporated onto a HOPG film. Squares: observed intensity ratio, full line: intensity ratio, assuming Rutherford cross section, dashed line: assumes ELSEPA cross sections [24]. The calculated lines were normalized to the experiment at 40 keV and a TPP-2M inelastic mean free path [27] was assumed.

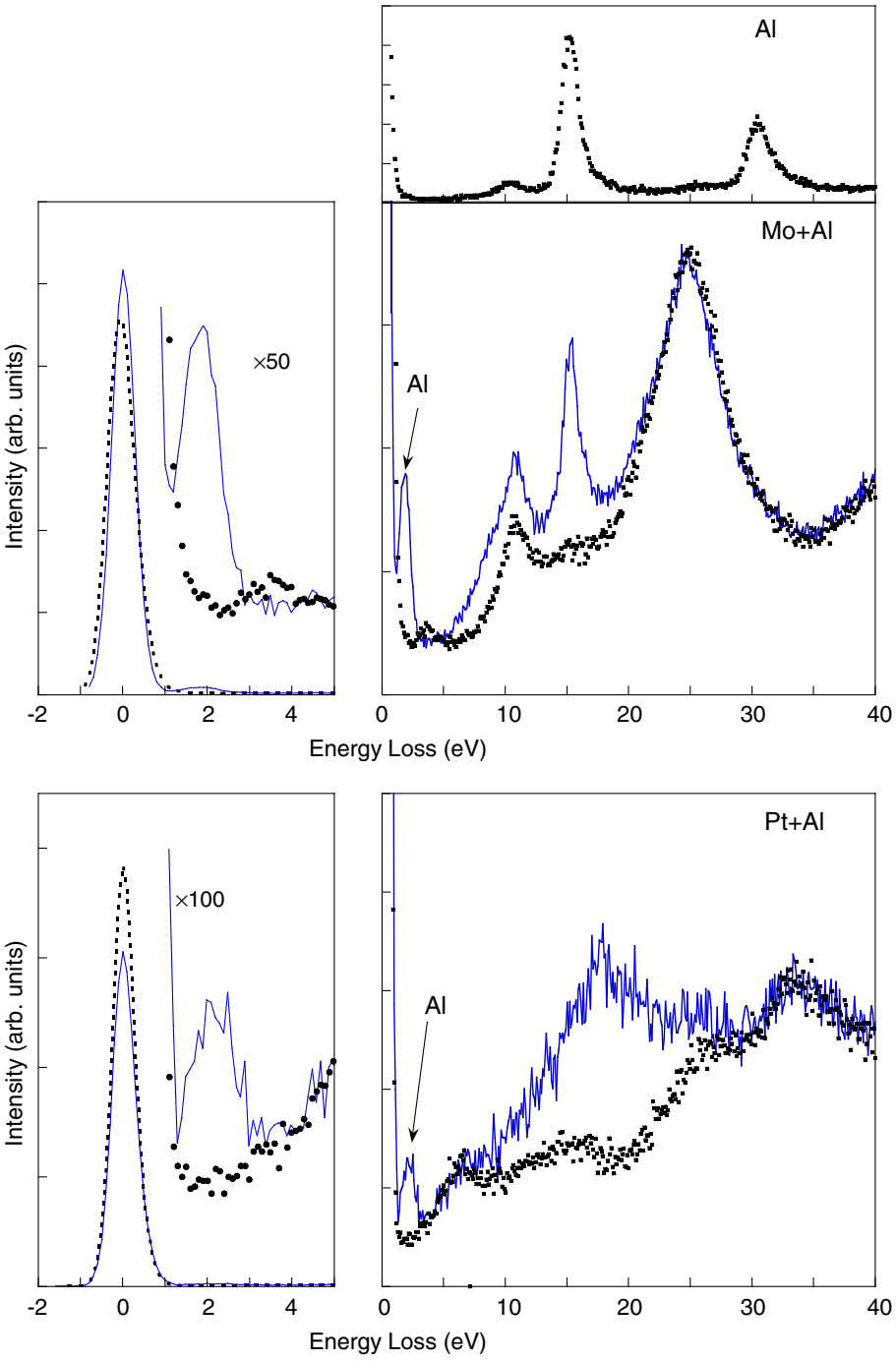

Fig. 9. Energy loss spectra, ($E_0 = 40$ keV) of Mo and Pt before (dotted) and after (lines) deposition of 80 Å Al. The top panel shows an Al energy-loss spectrum as a reference. After Al deposition a small Al elastic peak is visible besides the main substrate elastic peak (left panels). The energy loss spectrum of Al deposited on Mo resembles the sum of the Al and Mo loss spectrum. In contrast after deposition of Al on Pt, the spectrum has a broad feature near 17 eV, not present in either Pt or Al loss spectrum, implying that a reactive interface is formed.

energy-loss spectra can be explained as the sum of a Mo energy loss spectrum plus single-loss contributions (bulk and surface) of an Al metal overlayer.

The situation is completely different for the case of Pt. Now after the same thickness of Al is deposited, the Al peak is even smaller compared to the Pt peak. This is (at least in part) a consequence of the fact that the elastic-scattering cross section of Mo is smaller than the cross section of Pt. Again there are more significant changes in the energy-loss part of the spectrum. Now we do not see a sharp feature at 15.2 eV, but a much broader peak appears centered around 17 eV. We interpret this to indicate that Al reacts with Pt and that a surface layer is formed containing both Pt and Al.

In principle, one could test such an interpretation by calculating the loss function from ab initio methods [32], assuming a specific Pt–Al alloy, or one could determine these experimentally by measuring reference samples of Pt–Al alloys. After the loss function was established, one could try to simulate (probably using Monte Carlo methods) the measured spectra as presented here and describe the elastic and inelastic parts simultaneously in a quantitative way, using the loss functions and compositions of the layers involved as input parameters and their thicknesses as fitting parameters. Such an approach would be a critical test of our understanding of the interface formed, as it would be sensitive both to the electronic structure and elemental composition of the near-surface layers, but such an analysis has not been developed yet.

After deposition of more Al (total thickness ≈ 250 Å) on Pt, an Al plasmon becomes visible indicating that a pure Al film is being formed. With even more Al deposition, the Pt elastic signal becomes more and more attenuated and finally the Al and Pt elastic peaks have similar intensity. This situation is shown in Fig. 10 after deposition of 900 Å of Al. Most interestingly, the first and second plasmon peak appears split as well. All electrons that are detected have been deflected elastically by scattering either from Al or Pt, as excitation of a plasmon does not change the direction of a fast electron significantly. As the difference in recoil energy for electrons scattered from Pt and Al is larger than the plasmon width, we can still infer, even after the creation of one or two plasmons, if the electron scattered from Pt or Al as the two components of the plasmon peak are 15.2 eV separated from either the Al and Pt elastic peak. Note that the Pt elastic peak is smaller than the Al elastic peak; however, the plasmon component related to elastic scattering from Pt is larger than the plasmon component related to elastic scattering from Al. This is understandable as the electrons scattered from Pt have to transverse the whole Al layer, whereas electrons scattered from Al transverse only part of the Al layer. Thus with increasing energy loss the relative contribution of the component at larger depth increases. Details are discussed elsewhere [33].

9. Use of ERBS in applied physics

Now we have some insight in the processes that play a role in these ERBS experiments, let us conclude with an

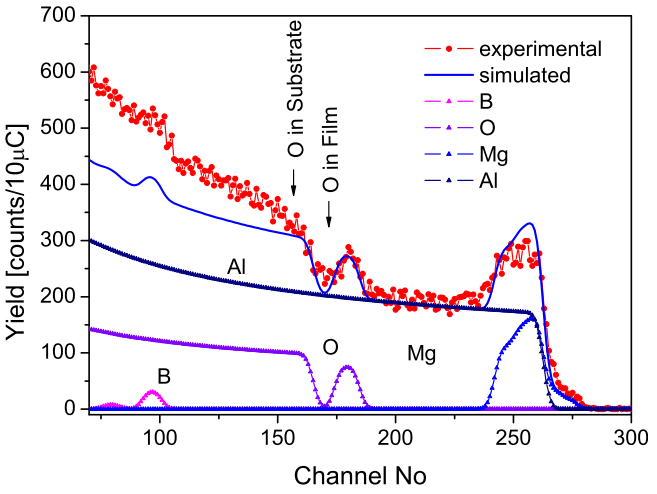

Fig. 11. A 2 MeV He^+ RBS spectrum of a MgB_2 film grown on alumina [34]. The scattering angle was 160° and the incoming beam was along the surface normal. The measured intensity is decomposed into contributions of different elements as indicated.

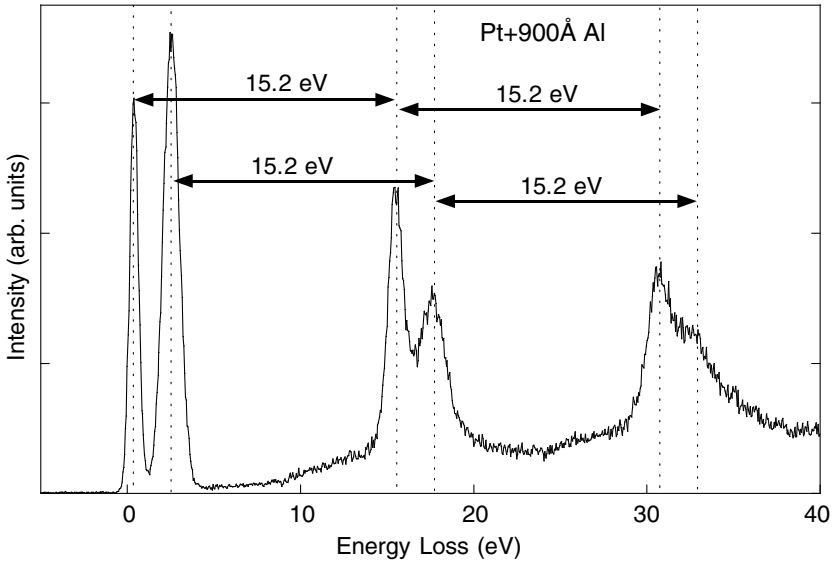

Fig. 10. The spectra after 900 Å Al was deposited on a Pt substrate. The Pt elastic peak is now somewhat smaller than the Al elastic peak. The Al plasmon is split as well, as the first (second) plasmon is at 15.2 eV (30.4 eV) lower energy compared to the corresponding elastic peak. The relative intensities of the plasmon components are inverted, reflecting the fact that electrons backscattered from Pt traverse the whole of the Al film, whereas electrons backscattered from Al traverse only part of this film.

example how this technique can be used as a surface analytical technique. In this example a thin film of the superconductor MgB_2 was grown on an Al_2O_3 substrate. These films, grown at the University of Wollongong by pulsed laser deposition, have good superconducting properties; see [34,35] for details. The resulting ion RBS spectrum taken at ANSTO laboratories in Sydney is shown in Fig. 11. The spectrum is fairly complex as it is a superposition of the signal from both the substrate and the overlayer film. Nevertheless it is clear that part of the overlayer contains oxygen. It is harder to ascertain if the oxygen is only at the surface or distributed through the whole film. Quantitative assessment of the amount of boron in the film is difficult too, as it is superimposed on a very large background.

The ERBS spectra of these films are shown in Fig. 12. A peak with a clear shoulder is seen, indicative of a second peak at somewhat larger energy loss. However the observed separation of the two peaks (1.4 eV) is smaller than the separation expected for Mg and B (3.5 eV). Both BN and MgO would have a separation between the two peaks close to 1.4 eV. If we knew the zero energy-loss position accurately, we could easily decide between both possibilities. However this position changes slightly with time. Hence the easiest way to establish which of the two possibilities is the correct one is to move the sample so the part of the electron beam hits the stainless steel sample holder. The Fe peak appears at a position consistent with that of the surface composition being MgO. Hence this is the correct interpretation of the as-received sample.

The surface layer was then removed by Xe ion sputtering. After sputtering 2 h using 1 keV Xe ions, we measure a decrease in the peak area of the oxygen and the first hint of some B contribution to the spectrum appears. The larg-

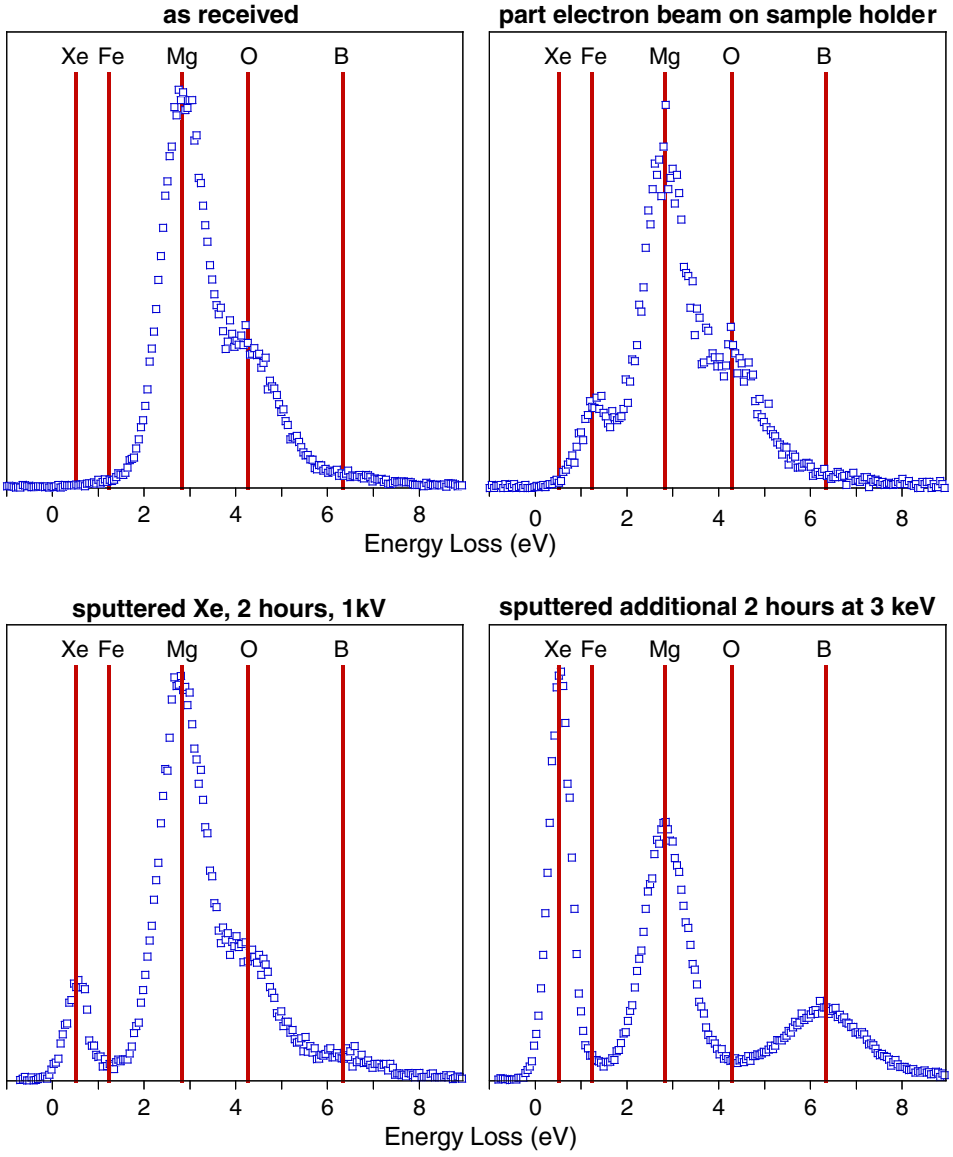

Fig. 12. The sequence of ERBS spectra, of a MgB_2 film as received and after sputtering, as described in the main text. The vertical bars indicate the calculated mean recoil energies $\overline{E_r}$ of the relevant elements.

est difference however, is the appearance of a new peak at very small energy loss. This is attributed to Xe implanted in the sample. Further sputtering for 2 h, now at 3 keV, seems to completely remove the oxygen layer, the B peak becomes well resolved and the Xe peak becomes more pronounced. Thus the subsurface composition of the film consists of Mg and B. The sputtering may have done damage to the film and change its composition and bonding. Hence analysis in terms of vibrational amplitude of Mg and B, as well as the stoichiometry was not done as these quantities are quite likely influenced by the sputtering process. Exposing the sample to air does not re-introduce the oxide layer, hence it was caused during thin-film growth in medium vacuum. We plan to determine the mean kinetic energy of Mg and B atoms and verify stoichiometry when films grown under UHV conditions, presumably without an oxide layer, become available.

Of course traditional ion beam experiments in combination with sputtering would probably also be able to show that no oxygen was present in the subsurface MgB_2 layer. This example is not intended to show that ERBS obtains information that can not be obtained in other way. It shows, however, that ERBS can provide non-trivial information in 'real-life' surface analysis. Another example of such a study is that of the oxide layer on Al films [36].

10. Summary and outlook

In this paper we sketched the underlying physics of high-energy electrons scattering over large angles from surfaces. A variety of factors (elastic and inelastic scattering cross sections, Doppler broadening, sample morphology) are of influence to the outcome. The successful interpretation of the spectra is a good test of our understanding of transport of keV electrons in solids. Results so far seems to indicate that interpretation is relatively straight forward, and there seems to be little doubt that, with increased experience, it can be developed as a technique that can provide unambiguous information about surface compositions with an intermediate surface sensitivity (100's of Å).

Is there a niche for this ERBS technique among the well-established tools in practical surface analysis such as Auger/XPS and RBS. This is a more difficult question. ERBS has some unique properties (bulk sensitive compared to XPS, compact compared to RBS, possible minimum spot size of electron beam compared to an ion beam, simultaneous information about the electronic structure and composition) that seem to suggest that indeed there might well be opportunities. We plan to further test our understanding of this technique and explore its possibilities in order to fully establish its merit as an analytical tool.

Acknowledgements

This research was made possible by a grant of the Australian Research Council. The authors want to thank R.G. Elliman for several ion backscattering measurements at the ANU, Y. Zhao (University Wollongong) and M. Ionescu (ANSTO) for the MgB_2 thin films and the corresponding RBS data and E. Weigold for critically reading the manuscript.

References

[1] W.K. Chu, Backscattering Spectrometry, Academic Press, New York, 1978.
[2] R.F. Egerton, Electron Energy-loss Spectroscopy in the Electron Microscope, second ed., Plenum Press, New York, 1996.
[3] M.R. Went, M. Vos, High-resolution study of quasi-elastic electron scattering from a two-layer system, Surf. Sci. 600 (10) (2006) 2070.
[4] M. Vos, M. Went, Elastic electron scattering at high momentum transfer: a possible new analytic tool, J. Elect. Spectros. Relat. Phenom. 155 (2007) 39.
[5] M. Vos, C.A. Chatzidimitriou-Dreismann, T. Abdul-Redah, J. Mayers, Electron and neutron scattering from polymer films at high momentum transfer, Nucl. Instr. and Meth. B 227 (2004) 233.
[6] A. Sosin, Energy dependence of electron damage in copper, Phys. Rev. 126 (5) (1962) 1698.
[7] H. Boersch, R. Wolter, H. Schoenebeck, Elastische energieverluste kristallgestreuter electronen, Z. Physik 199 (1967) 124.
[8] G. Gergely, M. Menyhárd, Z. Benedek, A. Sulyok, L. Kövér, J. Tóth, D. Varga, Z. Berényi, K. Tökési, Recoil broadening of the elastic peak in electron spectroscopy, Vacuum 61 (2001) 107.
[9] D. Varga, K. Tökési, Z. Berényi, J. Tóth, L. Körvér, G. Gergely, A. Sulyok, Energy shift and broadening of the spectra of electrons backscattered elastically from solid surfaces, Surf. Interf. Anal. 31 (2001) 1019.
[10] W.S.M. Werner, C. Tomastik, T. Cabela, G. Richter, H. Störi, Elastic electron reflection for determination of the inelastic mean free path of medium energy electrons in 24 elemental solids for energies between 50 and 3400 eV, J. Elect. Spectrosc. Relat. Phenom. 113 (2001) 127.
[11] W. Domcke, L. Cederbaum, Electronic recoil effects in high-energy photoelectron spectroscopy, J. Elect. Spectrosc. Relat. Phenom. 13 (1978) 161.
[12] R. Bonham, G. de Souza, Large angle elastic scattering from molecules: vibrational compton like scattering, J. Chem. Phys 79 (1983) 134.
[13] T. Fujikawa, R. Suzuki, L. Kövér, Theory of recoil effects of elastically scattered electrons and of photoelectrons, J. Elect. Spectrosc. Relat. Phenom. 151 (2006) 170.
[14] Y. Takata, Y. Kayanuma, M. Yabashi, K. Tamasaku, Y. Nishino, D. Miwa, Y. Harada, K. Horiba, S. Shin, S. Tanaka, E. Ikenaga, K. Kobayashi, Y. Senba, H. Ohashi, T. Ishikawa, Recoil effects of photoelectrons in a solid, Phys. Rev. B 75 (23) (2007) 233404.
[15] G.I. Watson, Neutron compton scattering, J. Phys.: Condens. Mater. 8 (1996) 5955.
[16] M. Vos, M.R. Went, Effects of bonding on the energy distribution of electrons scattered elastically at high momentum transfer, Phys. Rev. B 74 (2006) 205407.
[17] M. Vos, M.R. Went, Experimental confirmation of the EPES sampling depth paradox for overlayer/substrate systems, Surf. Sci. 601 (2007) 1536.
[18] W.H. Schulte, B.W. Busch, E. Garfunkel, T. Gustafsson, G. Schiwietz, P.L. Grande, Limitations to depth resolution in ion scattering experiments, Nucl. Instr. and Meth. B 183 (2001) 16.
[19] G. Placzek, The scattering of neutrons by systems of heavy nuclei, Phys. Rev. 86 (1952) 377.
[20] M.P. Paoli, R.S. Holt, Anisotropy in the atomic momentum distribution of pyrolitic graphite, J. Phys. C: Solid State Phys. 21 (1988) 3633.

[21] M. Berheide, W.H. Schulte, H.-W. Becker, L. Borucki, M. Buschmann, N. Piel, C. Rolfs, G.E. Mitchell, J.S. Schweitzer, Average kinetic energy of atoms in a solid measured with resonant nuclear reactions, Phys. Rev. B 58 (17) (1998) 11103.
[22] J. Mayers, T.M. Burke, R.J. Newport, Neutron Compton scattering for amorphous hydrogenated carbon, J. Phys.: Condens. Mater. 6 (1994) 641.
[23] A.L. Fielding, D.N. Timms, J. Mayer, Measurement of anisotropies of the kinetic energy and anharmonicity in pyrolitic graphite by neutron compton scattering, Europhys. Lett. 44 (2) (1998) 255.
[24] F. Salvat, A. Jablonski, C.J. Powell, ELSEPA dirac partial-wave calculation of elastic scattering of electrons and positrons by atoms, positive ions and molecules, Comput. Phys. Commun. 165 (2005) 157.
[25] M. Went, M. Vos, R.G. Elliman, Electron inelastic mean free path in solids as determined by electron Rutherford back-scattering, J. Elect. Spectrosc. Relat. Phenom. 156–158 (2007) 387.
[26] A. Jablonski, F. Salvat, C.J. Powell, Evaluation of elastic-scattering cross sections for electrons and positrons over a wide energy range, Surf. Interf. Anal. 37 (2005) 1115.
[27] S. Tanuma, C.J. Powell, D.R. Penn, Calculation of electron inelastic mean free paths, Surf. Interf. Anal. 20 (1993) 77.
[28] H. Hovel, T. Becker, A. Bettac, B. Reihl, M. Tschudy, E.J. Williams, Controlled cluster condensation into preformed nanometer-sized pits, J. Appl. Phys. 81 (1) (1997) 154.
[29] I. Lopez-Salido, D. Lim, Y. Kim, Ag nanoparticles on highly ordered pyrolytic graphite (HOPG) surfaces studied using STM and XPS, Surf. Sci. 588 (2005) 6.
[30] S. Tanuma, C.J. Powell, D.R. Penn, Calculations of electron inelastic mean free paths, Surf. Interf. Anal. 37 (2005) 1.
[31] M. Vos, M. Went, Metal interface formation studied by high-energy reflection energy loss spectroscopy and electron Rutherford back-scattering, Surf. Sci. 601 (2007) 4862.
[32] C. Ambrosch-Draxl, J.O. Sofo, Linear optical properties of solids within the full-potential linearized augmented planewave method, Comp. Phys. Commun. 17 (2006) 1.
[33] M. Vos, M. Went, Splitting the plasmon peak in high-energy reflection electron energy loss experiments, J. Elect. Spectros. Relat. Phenom. 162 (2008) 1.
[34] Y. Zhao, M. Ionescu, S. Dou, H. Liu, Study of oxygen incorporation in PLD MGB_2 films by Rutherford backscattering spectroscopy, IEEE Trans. Appl. Supercond. 17 (2007) 2875.
[35] Y. Zhao, Y. Wu, C. Kong, D. Wexler, M. Vos, M. Went, S.X. Dou, Phase evolution in PLD MgB2 films during the in situ annealing process, Supercond. Sci. Technol. 20 (2007) S467.
[36] M. Went, M. Vos, Electron Rutherford back-scattering case study: oxidation and ion implantation of aluminium foil, Surf. Interf. Anal. 39 (2007) 871.